Chapter 1

Introduction

The topical keyword for mass market RF applications is "wireless" - in terms of bi- and unidirectional communication and control. Recently, the wireless local area network (WLAN) and Bluetooth implementations are penetrating the market in a large variety of applications. The foundation for such a development are an international standardization process[1] in the forefield and an available license free frequency band. The *I*ndustrial-*S*cientific-*M*edical (ISM) band at 2.4 GHz, which is covering the frequency range from 2.4 GHz to 2.4835 GHz, is highly congested, already. To name only the most common applications in addition to the previously mentioned ones, microwave oven, sensor data transmission and remote control applications are located in this frequency range. There, jamming is a frequent condition. Manifold national restrictions in the 2.4 GHz band reduce the usable frequency range to a fraction of the available ISM band, which makes the present situation even more problematic.

On the other hand a wider available frequency band in combination with a low-cost analog RF front-end would open up more versatile applications. Very high data rate cable links, e.g. for video applications, might be replaced by wireless connectors. A short range wireless stack to the IEEE 1394 bus interface (see link [5]) is also a potential mass market application to replace the so called "firewire" cable.

Another possible high volume market is the area of sensor applications. All electronic devices can be made "user aware" if needed by equipping them with a simple radar sensor. The recent developments in the automotive sector is delivering a great demand for low cost radar sensors. The electronic ambient awareness of luxury cars with low market volume should be integrated in high market volume lower class cars, also.

An current keyword in research and development is "ambient intelligence", which is expected to deliver the next drive to the RF industry. In such an ambient, electronic devices with computational capability are linked to a dynamic network. They are equipped with sensors collecting information from the ambient and are capable to interact "intelligently" with the ambient thru actuators. These applications will drive the need for low-cost sensor and compact wireless communication units.

There are several license free frequency bands for the applications mentioned above. Lower than 1 GHz they are highly occupied by amateur radio and wireless device communication applications, already. There, the available modulation bandwidth of less than 30 MHz additionally split in several channels makes a high data rate communication in the MBit/s range impossible. The ISM bands above 1 GHz are besides the widely used 2.4 GHz, the 24 GHz ($24 - 24.25$ GHz) and 61 GHz ($61 - 61.5$ GHz) bands. Above 100 GHz there are two more assigned bands ($122 - 123$ GHz and $244 - 246$ GHz). However, these frequencies cannot be covered by the performance of the present MMIC technologies, or addressed by low-cost solutions. For wireless local area network applications, there exists a license free frequency allocation at 5 GHz ($5.15 - 535$ GHz and $5.47 - 5.725$ GHz). Due to its restriction to these applications only, this frequency band is not of interest for the present work.

[1] like the international standard IEEE 802.11 (see link [3]) together with the interoperability certification framework provided by the nonprofit Wi-Fi alliance (see link [4]).

The move to 24 GHz has several advantages. Antenna geometries shrink to a few millimeters, allowable data rates increase, and the potential for interference with other electronic equipment decreases significantly. The higher radiation absorption in walls and other obstacles allows a more frequent re-use of the frequency of operation. Likewise, the penetration depth into biological tissue is also reduced dramatically due to the skin effect, addressing the widespread fears of unknown non-thermal interactions of electromagnetic radiation with biological matter, most notably the interior milieu of cells. Even more this is valid for 61 GHz, but at the starting point of this work no low-cost MMIC technology delivering the required performance was available. At the present time the Silicon based MMIC technologies suitable for a high integration level at 60 GHz and above have the production status.

Today, many technologies adequate to meet RF system specifications of a 24 GHz analog front-end IC are available. Advanced pure Silicon digital CMOS processes with 90 nm feature size can be used for 24 GHz analog applications, already. The high performance is accompanied by very high initial setup costs of this technology, caused by the high-resolution mask-set. This condition makes research activity, which also needs design iterations, even more cost-intensive. Traditional III-V technologies are designed for single-function designs using distributed elements, and rarely have more than two metalization levels (including air bridges). The distributed element approach using transmission lines instead of concentrated elements as spiral inductors and capacitors increases the chip size and prevents low-cost solutions. On the other hand the thermal resistance of GaAs, which is three times higher than that of Silicon, already limits integration density. A Silicon based heterojunction bipolar MMIC technology using Silicon-Germanium alloy in the base layer of the transistors is providing high RF performance at a relaxed μm-scale feature size. Together with a multi-level metal system and high thermal conductivity substrate it is providing a good fundamental for highly integrated millimeter-wave circuits.

Increasing the operation frequency is accompanied by elevated electrical and thereby mechanical accuracy requirements for the chip interconnects, which is driving the system cost. Reducing the component count and increasing the integration level paves the way to low-cost solutions. In this work, a fully integrated 24 GHz module has been evaluated, which includes the transmitting and receiving antenna elements on-chip. This integration level highly releases the chip interface connection requirement due to only the low intermediate frequency and DC supply connections to the chip. A high integration level on Silicon substrate at 24 GHz comes along with increased crosstalk within the IC. The coupling paths within the substrate and the metal system must be analyzed. In this work, on-chip coupling is reduced by targeted design concepts which improve isolation.

Chapter 2

Proposed Application

This work evaluates, develops and demonstrates a fully integrated analog front-end for wireless communication applications in the 24 GHz ISM band, for which the transmit and receive antenna is integrated on-chip, also.

2.1 Link Budget

The system specifications are discussed based on a link budget under the following assumptions:

- The communication range is comparable to Bluetooth class 2 (10 m). The transceiver system should replace a high speed wire based connection between a host and a client system
- The digital modulation format QPSK (Quaternary Phase Shift Keying) is a compromise between high spectral efficiency and an acceptable bit error rate at low signal-to-noise ratio. This modulation format's signal-to-noise ratio at a worst case bit error rate of 10^{-6} is used to evaluate the link performance depending on the link distance
- Low-directivity antennas are assumed, which can also be realized on-chip leading to a significant simplification in packaging.

2.1.1 Digital Modulation Format

Setting up a link budget [6] starts with determining the signal-to-noise ratio (SNR) needed to demodulate a received signal with a given modulation format and bit error rate. It is the minimum power ratio to achieve between the wanted received signal power S^* and the noise power N^* (thermal noise, interfering noise due to other transmitters on the same frequency band). It is defined as

$$\frac{S}{N} = 10\log_{10}\left(\frac{S^*_{\text{Power}}}{N^*_{\text{Power}}}\right). \tag{2.1}$$

Based on the acceptable Bit-Error-Rate (BER =Bits in Error/Total Bits received) in a receive system, the required corresponding SNR can be calculated. The Quaternary Phase Shift Keying (QPSK) format is taken here as a representative of a simple digital modulation format, which has a theoretical spectral efficiency[1] of 2 bit/s/Hz. The carrier's phase is modulated in 90^0 steps, by which one symbol transmits 2 bits [7]. The probability of error of QPSK is calculated from:

$$P_{\text{e}} = \frac{1}{2}\text{erfc}\left(\sqrt{\frac{E_{\text{b}}}{N^*_0}}\right), \tag{2.2}$$

[1] In practice, the efficiency is limited by the filters roll-off factor. With a roll-off factor of 0.2 the spectral efficiency is 0.83 bit/s/Hz

where E_b is the energy per bit and N_0^* is the noise power density, which is given by:

$$N_0^* = k \cdot T_0 = 4.0 \cdot 10^{-21} \mathrm{W/\,Hz}. \tag{2.3}$$

The more common used expression is in decibels with: $N_0 = 10 \cdot \log_{10}(N_0^*) = -174\,\mathrm{dBm/\,Hz}$. The absolute noise power within the bandwidth occupied by the signal is calculated from:

$$N^* = N_0^* B_\mathrm{n}, \tag{2.4}$$

where B_n is the noise bandwidth. For QPSK the energy per bit (E_b) is

$$E_\mathrm{b} = \frac{E_\mathrm{s}}{2}, \tag{2.5}$$

where E_s is the energy per symbol, with

$$B_\mathrm{n} = \frac{R_\mathrm{b}}{2}, \tag{2.6}$$

where B_n is the noise bandwidth and R_b is the bit rate. Therefore,

$$\frac{E_\mathrm{b}}{N_0^*} = \frac{C^*}{R_\mathrm{b}} \cdot \frac{B_\mathrm{n}}{N^*} = \frac{C^*}{2N^*}, \tag{2.7}$$

and Equation 2.2 can be rewritten as:

$$P_\mathrm{e} = \frac{1}{2}\mathrm{erfc}\left(\sqrt{\frac{1}{2}\frac{C^*}{N^*}}\right), \tag{2.8}$$

which relates the error probability to the carrier-to-noise power ratio (C^*/N^*). Figure 2.1 depicts the probability of error calculated from Equation 2.8.

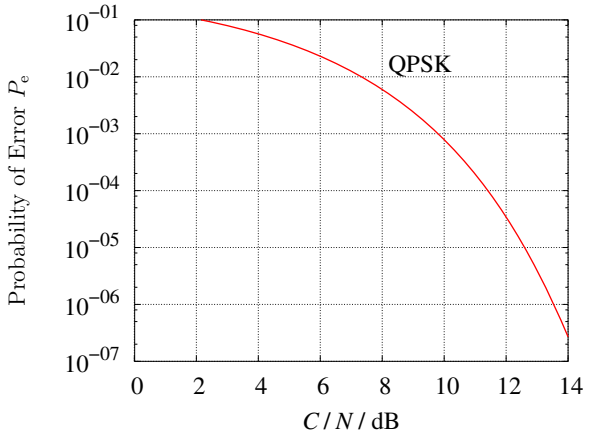

Figure 2.1: Probability of error for QPSK

A typical value for P_e for wireless Rx systems to refer their input sensitivity is 10^{-6} in the literature. At this error probability the required carrier-to-noise ratio is 13.5 dB. Commercial signal demodulators in base-band exhibit demodulation losses in the range of 0.5 dB with respect to theory at $E_\mathrm{b}/N_0 = 1\,\mathrm{dB}$ ($C/N = 4\,\mathrm{dB}$ for QPSK). Therefore, a required SNR of 14 dB is taken for link budget calculations in the next section.

2.1.2 Link Budget Calculations

Noise Figure

The noise figure F indicates the decrease in SNR between the input and the output of a system:

$$F^* = \frac{SNR^*_{\text{in}}}{SNR^*_{\text{out}}} = \frac{\frac{S^*_{\text{in}}}{N^*_{\text{in}}}}{\frac{G^* \cdot S^*_{\text{in}}}{G^* \cdot \left(N^*_{\text{in}} + N^*_{\text{ai}}\right)}} = \frac{N^*_{\text{in}} + N^*_{\text{ai}}}{N^*_{\text{out}}} = 1 + \frac{N^*_{\text{ai}}}{N^*_{\text{in}}}, \tag{2.9}$$

where S_{in} is the signal power density, N_{in} is the noise power density at the input, G^* is the system gain and N^*_{ai} the systems artificial noise power density at the input. To make the noise figure comparable, it is referenced to the noise power density N^*_0 of a resistor at $T_0 = 290\,\text{K}$ (see Equation 2.3). In other words, an amplifier with $F = 3\,\text{dB}$ decreases the signal-to-noise ratio by 3 dB, if the incoming noise power density is N^*_0 (the source temperature is 290 K).

Friis Equation

The transmitted power with arbitrary antenna gain is given by:

$$P^*_{\text{Tx}} = P^*_{\text{out}} G^*_{\text{Tx}}, \tag{2.10}$$

with the available output power P^*_{out} at the systems output port and the transmitter antenna gain G^*_{Tx}.
The line-of-site loss is:

$$L^*_{\text{p}} = \left(\frac{4\pi}{c} f d\right)^n, \tag{2.11}$$

where the exponent n is 2 for free space, with the distance d separating Tx and Rx antennas, the frequency f, the speed of light c. In-door propagation experiments have been performed at the California Institute of Technology [8], also at 24 GHz. Under the conditions of their indoor environment, they determined a Line-of-Site path loss exponent of 1.7, which indicates a side wall guiding effect. In the case of their Non-Line-of-Sight path loss experiments an exponent of 2.1 has been determined, which promises only a slightly higher path loss compared to the free space condition. The distinct guiding effect of the walls could be explained by the wave length of 1.5 cm at 24 GHz. Even small metallic matter acts as a reflector at 24 GHz and increases the reflectivity of the walls. For the link-budget calculations here, the loss exponent is taken to be 2. A 10 m transmission distance corresponds to $L_{\text{p}} = 80\,\text{dB}$ at 24 GHz.

Received power with arbitrary antenna gain is given by the Friis equation:

$$P^*_{\text{Rx}} = \frac{P^*_{\text{Tx}} G^*_{\text{Tx}} G^*_{\text{Rx}}}{L^*_{\text{p}}}, \tag{2.12}$$

with the receiver antenna gain G^*_{Rx}.

The antenna used in this work is of dipole type, which is realized on-wafer on a 1000 Ωcm Silicon substrate. The theoretical directivity of a full size half wave dipole is $G = 2.1\,\text{dBi}$. A prototype sample has delivered a measured gain of $-1\,\text{dBi}$ [9].

Now, the maximum modulation bandwidth can be calculated as a function of the targeted link distance d from the Equations 2.4, 2.8, 2.10, 2.11 and 2.12, the maximum deliverable power of $P_{\text{out}} = 7\,\text{dBm}$ in Tx (see Section 5.1.4), the receiver's noise figure of $F_{\text{receiver}} = 7\,\text{dB}$ (see Section 5.6) and the gain of the on-wafer antenna of $G_{\text{Tx,Rx}} = -1\,\text{dBi}$. The relation between maximum modulation bandwidth, which is set to be equal to the noise bandwidth B_{n}, and link distance d is calculated from:

$$B_{\mathrm{n}} = (P_{\mathrm{out}} + G_{\mathrm{Tx}} + G_{\mathrm{Rx}}) - L_{\mathrm{p}} - N_0 - F_{\mathrm{receiver}} - SNR_{\mathrm{min}} - m_{\mathrm{sys}} \tag{2.13}$$

where, SNR_{min} is the minimal SNR at the demodulator input and m_{sys} is the system margin. The Equation 2.13 (B_{n}^{*}) is plotted in Figure 2.2 for $SNR_{\mathrm{min}} = 14\,\mathrm{dB}$ (see Section 2.1.1) and a system margin (m_{sys}) of 3 dB.

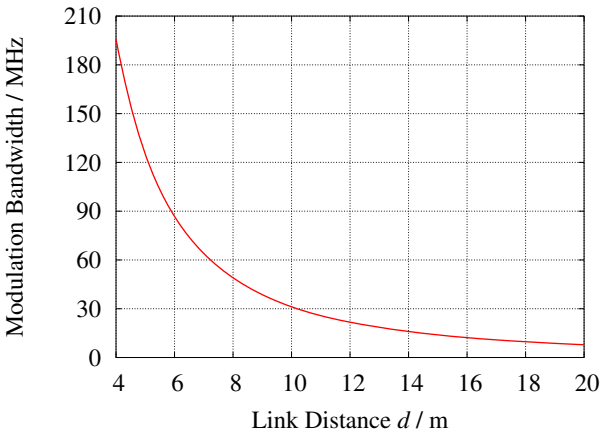

Figure 2.2: Maximum modulation bandwidth as a function of the link distance d with $SNR_{\mathrm{min}} = 14\,\mathrm{dB}$ and $m_{\mathrm{sys}} = 3\,\mathrm{dB}$

It can be seen from this diagram that a link distance of 10 m allows a modulation bandwidth of 30 MHz. On the other hand, for close vicinity application ($d < 4\,\mathrm{m}$) the usable bandwidth is $>$ 180 MHz, which corresponds to a (gross) bit rate $> 360\,\mathrm{Mbit/s}$.

Atmospheric Absorption

Millimeter waves are absorbed in the atmosphere depending to their wavelength mainly due to the absorption by: oxygen (O_2) and water vapor (H_2O). Because absorption is proportional to the absolute humidity, the graph shown in Figure 2.3 is adjusted to be representative of a water content of $7.5\mathrm{g/\,m^3}$ at 20°C It has been adopted from [10].

There is an absorption minimum at 35 GHz between about 22 GHz and 60 GHz, which are the absorption bands of H_2O and O_2, respectively. 24 GHz is close to a peak in the water spectrum. In [11], the 20-32 GHz frequency range has been analyzed more accurately. The attenuation is measured to be $0.147\,\mathrm{dB/\,km}$, which makes this loss mechanism irrelevant for close range applications. The atmosphere becomes progressively more opaque at higher frequencies, with windows at 94, 140 and 220 GHz for frequencies below 300 GHz between the O_2 and H_2O lines.

2.2 Transceiver Topologies

In wireless receive and transmit systems, the analog front-end at the carrier frequency is the most demanding circuit part in terms of current consumption, technology performance-demands and sensitivity to parasitics. For the frequency down conversion the superheterodyne-technique is applied here, which has been invented by Edwin Howard Armstrong and patented in 1918. Compared to superheterodyne a direct-conversion concept would further reduce the overall component count for a receive system and the choice of an sub-harmonically pumped frequency conversion topology would additionally prevents the LO signal to be converted to DC by self-mixing [12] due to $f_{\mathrm{LO}} = f_{\mathrm{RF}}/2$. This approach would give the advantage to design the on-chip oscillator at lower frequencies, which delivers the potential to achieve a lower phase noise for a given concept and technology. These advantages are paid by a higher component count at RF.

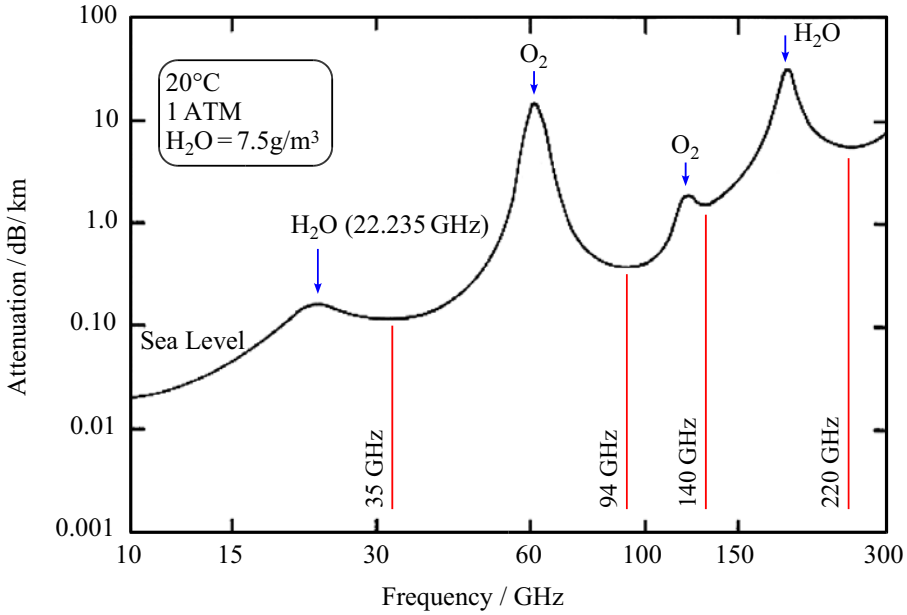

Figure 2.3: Average atmospheric clear weather absorption of millimeter waves for horizontal propagation as a function of frequency (adopted from [10])

For converting down to an IF, the image RF must be either filtered before entering the mixer or inherently suppressed by an appropriate technique to prevent being converted down to the same IF, which is an additional noise contribution. In case of low IF applications (200 MHz), an image frequency filter must have a high quality factor Q and a steep filter edge, which cannot be integrated using lumped components for the filter due to the low Q of the on-chip inductors (see Section 3.3). Integrated filters with high Q can be realized by applying distributed concepts, as described in [13], but has not been chosen here, due to their large extensions, preventing low cost fully integrated solutions. Here, the image cancellation approach is chosen, because the RF critical components can be fully integrated. From the fully integration point of view, it is advantageous to rather design the mixer active than passive. Active mixer concepts need a lower local oscillator power compared to passive designs. This property is reducing the effort for designing a high power integrated oscillator. Additionally, an active mixer is delivering conversion gain, which need not to be delivered by the subsequent IF stages. On the other hand an active mixer approach has mostly a higher RF noise than for passive mixers. To cope with lower system noise figure requirements than the mixer is delivering, a low noise amplifying stage in front of the mixer is needed to make its noise contribution negligible.

Because a single-ended design at the high frequency of 24 GHz leads invariably to problems with common-node impedance, a differential design was chosen. This is discussed in detail in Section 4.2.

From these requirements, the topology shown in Figure 2.4 was chosen to evaluate the fully integrated front-end.

The receiver antenna's RF signal is fed to a low noise amplifier first, which is amplifying the usually weak signal power by adding only a minimal noise power. The LNA is discussed in Section 5.1 in detail. The image reject mixer consisting of the two mixer blocks, LO poly-phase filter, low-pass filter and the IF buffer is discussed in Section 5.2. The local oscillator signal generation is discussed in Section 5.3.

To stabilize the local oscillator's operation frequency its phase is locked by an off-chip circuitry to the phase of a stable fixed-frequency oscillator. Commercially available low-cost PLLs operate in the frequency range between $1 - 2$ GHz. Therefore, the oscillator's frequency of 24 GHz is divided down to that range by a frequency divider (also called prescaler), which is discussed in Section 5.4.

The function blocks within the dashed box are either operating at RF frequencies or are not bulky in terms of their component extension on the wafer. Therefore, they are suitable to be integrated on a

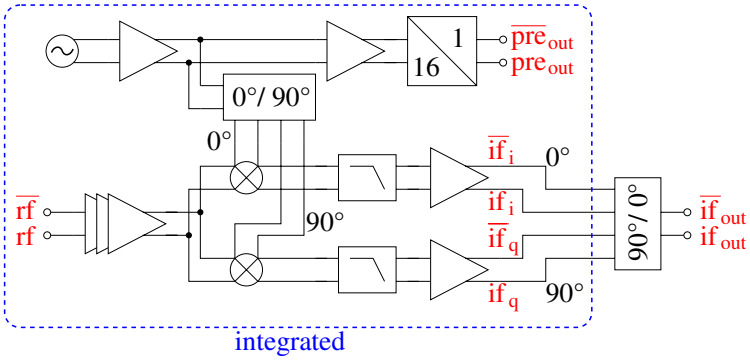

Figure 2.4: Receiver block diagram

single chip. The 90^0 phase shifter, which is operating at the intermediate frequency, is designed not to be integrated into the front-end due to its larger extension, and because its interface connection properties at lower frequencies are not critical.

It is possible to realize a transmitter by reusing the function blocks of the receiver depicted in Figure 2.4. The rearranged function blocks can be seen in Figure 2.5.

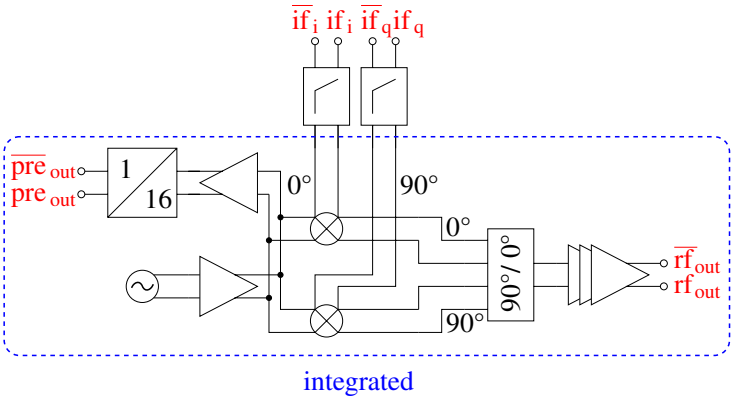

Figure 2.5: Transmitter block diagram

This way of designing a different system with new overall functions, based on function blocks used in other circuits, on the other hand, is very common in the digital domain. The design reuse in the analog domain is mainly suffering from a function block's performance dependence on its direct on-chip environment. The design approach common for all function blocks used in this work and their dependence on the electrical and on-chip environment are discussed in detail in Chapter 4, which is presenting a set of techniques to overcome the on-chip environmental dependencies. The underlying MMIC technology is described in the next chapter.